OPEN ACCESS
IOP Publishing | Astro Ltd
Laser Physics
Laser Phys. **29** (2019) 035701 (6pp)
https://doi.org/10.1088/1555-6611/aaffcb

Detuning radio-frequency electrometry using Rydberg atoms in a room-temperature vapor cell

Linjie Zhang[1,2,4], Yue Jia[1,2], Mingyong Jing[1,2], Liping Guo[3], Hao Zhang[1,2], Liantuan Xiao[1,2] and Suotang Jia[1,2]

[1] State Key Laboratory of Quantum Optics and Quantum Optics Devices, Institute of Laser Spectroscopy, Shanxi University, Taiyuan 030006, People's Republic of China
[2] Collaborative Innovation Center of Extreme Optics, Shanxi University, Taiyuan, Shanxi 030006, People's Republic of China
[3] College of Physics and Electronics, Shanxi University, Taiyuan, 030006 Shanxi, People's Republic of China

E-mail: zlj@sxu.edu.cn

Received 9 May 2018, revised 11 July 2018
Accepted for publication 1 January 2019
Published 19 February 2019

Abstract

Traceable radio-frequency electric field measurements with high sensitivity have been demonstrated from the centimeter wave to the millimeter wave using room-temperature Rydberg atoms. Here, we investigate the splitting spectra of electromagnetically induced transparency induced by a radio-frequency electric field, which is detuned from the resonant frequency of transitions between two Rydberg states, $47D_{5/2} \leftrightarrow 48P_{3/2}$. By varying the detuning of the radio-frequency electric field, we measure the separation between the two peaks, and in particular their relative height. The resulting measured resonant transition frequency between two Rydberg states is found to exhibit a visible change when the power of the radio-frequency electric field is varied, thus causing uncertainty in the traceable radio-frequency electric field measurement. Further, the effect of detuning of the probe light on the radio-frequency electric field measurement is presented.

Keywords: Rydberg atom, radio-frequency electric field measurement, electromagnetically induced transparency

(Some figures may appear in colour only in the online journal)

1. Introduction

Rydberg atoms are highly excited atoms with a large principal quantum number. Compared with the ground state atoms, Rydberg atoms have a large orbital radius and large dipole moment [1], and are very sensitive to the external electric field [2, 3]. Electromagnetically induced transparency (EIT) is a phenomenon where the transmission of a weak probe field increases in an absorbing medium when a strong coupling field is used [4]. The effect of EIT is widely used in nonlinearity enhancement [5, 6], electric dipole moment measurements [7, 8], optical quantum storage [9, 10] and other aspects.

Rydberg EIT has been used to measure radio-frequency electric-field (RF E-field) strengths over a large range of frequencies (1 GHz to 500 GHz) by using a room-temperature vapor cell [11–16]. An RF E-field applied to the Rydberg atoms results in the Autler–Townes (AT) splitting of the Rydberg EIT transmission spectrum. Using this approach, RF E-fields can be measured with a high sensitivity, approximately 30 μV cm^{-1} Hz$^{-1/2}$ [12]. Millimeter wave E-field spatial distributions have recently been demonstrated with a high resolution

[4] Author to whom any correspondence should be addressed.

of approximately $\lambda/650$ [14, 15], where λ is the wavelength of the millimeter E-field. The polarization of RF E-fields was also identified; the resolution of polarization reached 0.5° [13]. As a core component of RF E-field electrometry, the effects of the size of the vapor cell on the accuracy of the measurements was investigated [16]. Simons *et al* demonstrated the improved measurement sensitivity of a weak detuning RF E-field strength compared to an on-resonant RF electric field [17].

In this work, we investigated the EIT-AT spectrum of a ladder four-level system involving Rydberg states in a room-temperature vapor under the condition of the detuning RF E-field and a probe light. The splitting separation and the relative height ratio of two peaks of the AT spectra are presented respectively as a function of the frequency detuning and the power of the RF E-field. It is shown that the power of the RF E-field will cause the frequency shift of the $47D_{5/2}$-$48P_{3/2}$ Rydberg transition. The model of a four-level system theory is used and provides a good qualitative explanation for the experimental observation. Moreover, the effect of the EIT-AT splitting on the detuning of the probe light is demonstrated.

2. Experimental approach

Figure 1(a) is the four-level atomic energy level scheme in our experiments. In a typical three-level EIT system, a 'dark state' is created by a probe field (Ω_p) and a coupling field (Ω_c), which prevent the resonant absorption of the probe laser. An applied RF field that is resonant with the two adjacent Rydberg states breaks down the three-level system and causes the probe photons to be absorbed again. The EIT spectrum will split into two peaks: this is called AT splitting. The AT splitting (Δf) is proportional to the RF E-field strength E and is described as

$$E = \Omega_M = \frac{2\pi\hbar}{\wp_{MW}}\Delta f \tag{1}$$

where $\wp_{MW}$ is the transition dipole moment of the adjacent Rydberg states and $\hbar$ is Planck's constant, and Ω_M is the Rabi frequency of the Rydberg state transition induced by the RF E-field [18].

Figure 1(b) shows the experimental setup. We use a cylindrical vapor cell with 50 mm length and 20 mm diameter containing cesium (^{133}Cs) atom vapor. The probe laser drives the $6S_{1/2}(F = 4) \rightarrow 6P_{3/2}(F' = 5)$ transition and is generated with an external cavity diode laser. To observe an EIT signal, we apply a counter-propagating coupling laser (~510 nm) with a scanning frequency near the transition between $6P_{3/2}$ and $47D_{5/2}$. The coupling laser (Toptica TA-SHG110) is supplied by a frequency doubled amplified diode laser at 1020 nm. The Rabi frequency of the probe (coupling) laser is $\Omega_p = 8.08$ MHz $\times 2\pi$ ($\Omega_c = 2.05$ MHz $\times 2\pi$). Both lasers have the same linear polarization and are locked to a high-finesse Fabry–Pérot cavity made by the ultra-low-expansion glasses. Each laser has a spectral bandwidth less than 1 kHz according to the cavity transmission linewidth. It is necessary to shift the laser frequency to the resonance transition by the double-passed acoustic-optical modulator (AOM). The RF E-field at about 6.946 GHz, which couples resonantly to the transition of $47D_{5/2} \leftrightarrow 48P_{3/2}$, is led into the vapor cell by a horn antenna. The frequency of the coupling laser is scanned by an AOM so that the precise frequency of the splitting interval can be obtained. Meanwhile, the laser power is stabilized by a proportion-integral-differential feedback loop system by controlling the AOM diffraction efficiency to reduce the intensity noise.

3. Experimental results and discussion

The EIT signal and AT splitting spectrum of the probe transmission induced by an RF E-field are shown in figure 2(a). Figure 2(b) shows the signals under the detuning of the RF E-field. The splitting peaks in the upper figure show almost equal heights for the near-resonance RF E-field. The other signals in the lower part of figure 2(b) show the asymmetric height of the splitting peaks under the detuning frequency ±5 MHz. Taking into account the relation between the splitting and Rabi frequency of the RF transition in equation (1), the splitting separation can be given by

$$\Delta f = \sqrt{(\Delta_M)^2 + (\Delta f_0)^2}, \tag{2}$$

where $\Delta_M = f - f_0$ is the frequency detuning of the RF E-field, f is the measured E-field frequency, f_0 is the resonance frequency of the $47D_{5/2} \leftrightarrow 48P_{3/2}$ transition. Here, Δf_0 is the splitting interval induced by the resonant RF E-field and is equal to the Rabi frequency of the RF resonance transition in our experimental configuration. The RF E-field with the resonance frequency has the minimum AT splitting. Figure 3(a) shows the dependence of the splitting interval Δf on the absolute radio frequency f. The simulation curves using equation (2) are shown with the solid lines. The Rabi frequency on the Rydberg resonance transition equal to $2\pi \times (5.187 \pm 0.4$ MHz), $2\pi \times (6.732 \pm 0.21$ MHz), $2\pi \times (8.356 \pm 0.1$ MHz), $2\pi \times (10.386 \pm 0.06$ MHz) and $2\pi \times (12.952 \pm 0.05$ MHz) corresponds to the different output power of the RF generator: −21 dbm, −19 dbm, −17 dbm, −15 dbm and −13 dbm, respectively. The RF E-field strength can be calculated by the splitting Δf_0 using equation (1): for example, the RF E-field strength equals 19.86 ± 1.53 mV cm^{-1} for the on-resonant AT splitting of $2\pi \times (5.187 \pm 0.4$ MHz). The detuning RF E-field would cause larger splitting and improve the measurement sensitivity than that of the resonance frequency [17]. Moreover, the splitting measurement can offer a method to obtain the resonance frequency of the Rydberg transition through equation (2).

However, the simulation results of the resonance frequency for the different RF E-field strength in figure 3(a) is shown in figure 3(b). It is noted that the resonance frequency shifts with the variation in RF E-field strength, which is similar to the effect of the molecule photo-association [19]. The RF E-field induced the frequency shift of the resonance transition between Rydberg states. Here, the induced frequency shift is smaller than 0.3 MHz according to the mean values in figure 3(b). Considering the error of the fitting results, the maximum frequency shift is about 1.2 MHz.

To investigate the frequency shift with the power of detuning RF E-fields in detail, we illustrate the relation of the height

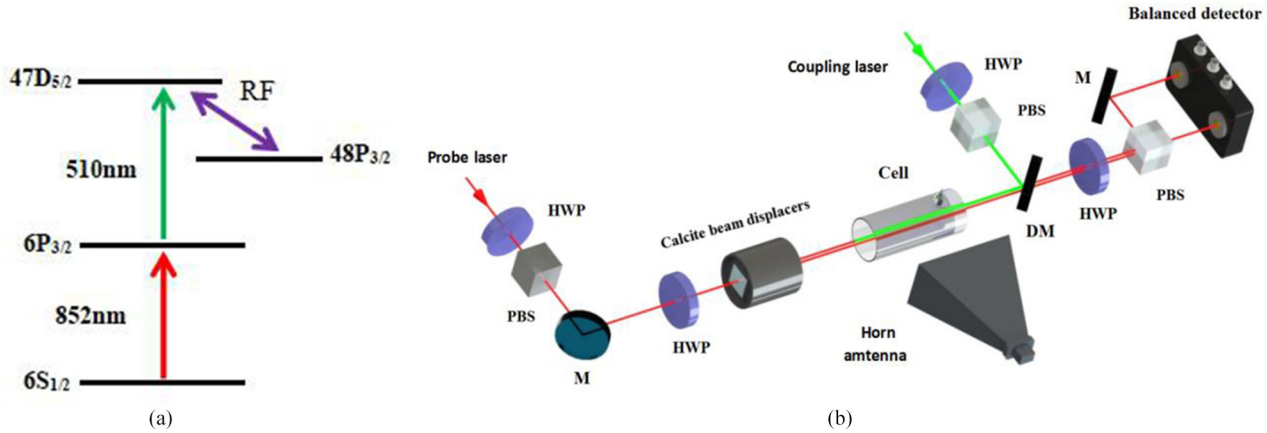

(a) (b)

Figure 1. (a) An energy-level diagram for Rydberg EIT and the Rydberg states coupled by RF fields. The 852 nm and 510 nm lasers are the EIT probe and coupling lasers, respectively. The RF E-field couples to the $47D_{5/2}$-$48P_{3/2}$ transitions. (b) An illustration of the experimental setup (HWP: half-wave plate, PBS: polarization beam splitter, DM: dichroic mirror and M: mirror). The transmission of the probe beam through the cell is monitored on a balanced detector.

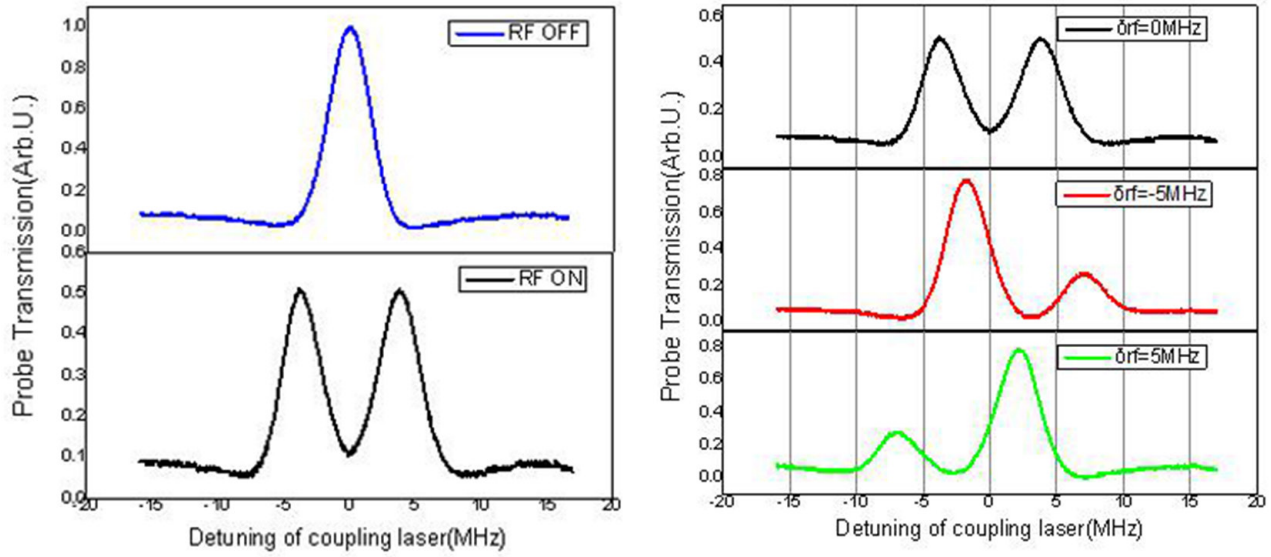

(a) (b)

Figure 2. (a) The EIT transmission signal without the RF E-field and the EIT splitting spectrum when an RF E-field was applied. (b) The EIT signal for the output power of an RF generator of −13 dBm and $\delta f = +5$ MHz, 0, −5 MHz.

ratio of two AT splitting peaks to the detuning of the E-field frequency. The radio frequency is varied in a small range from 6.9455 GHz to 6.9485 GHz. In figure 4(a), we show the height ratio of right peak H_2 to left peak H_1 of AT splitting curves for the different radio frequencies with the selected output power: −13 dbm, −15 dbm, −17 dbm, −19 dbm and −21 dbm. Figure 4(a) shows the slope of the height ratio is dependent on the applied RF E-field power. The smaller RF power produces the bigger slope. The curves corresponding to the variation in RF power intersect at a resonant frequency when the height ratio of the AT splitting peaks is equal to 1. It is noted that the frequency shift is about 1.1MHz under the different RF E-field power. Figure 4(b) shows the theoretical simulation curves for the four-level ladder system, which is similar to [20]. Here, the frequency shift induced by the RF E-field is not considered. The Hamiltonian matrix of the four-level ladder system is given:

$$H = \frac{\hbar}{2}\begin{bmatrix} 2\Delta_p & \Omega_p & 0 & 0 \\ \Omega_p & 0 & \Omega_c & 0 \\ 0 & \Omega_c & 2\Delta_c & \Omega_M e^{-i\phi} \\ 0 & 0 & \Omega_M e^{i\phi} & 2\Delta_M \end{bmatrix}, \tag{3}$$

where Ω_p, Ω_c, Ω_M are the Rabi frequency corresponding to the probe laser, coupling laser and the RF E-field, respectively, φ is the initial phase of the RF E-field. Here, Δ_p, Δ_c and Δ_M are the detuning associated with the probe, coupling and RF E-field corresponding to the transition of states, respectively. The master equations are given as

$$\dot{\rho}_{ij} = -\frac{i}{\hbar}\sum_k (H_{ik}\rho_{kj} - \rho_{ik}H_{kj}) - \frac{1}{2}\sum_k (\Gamma_{ik}\rho_{kj} + \rho_{ik}\Gamma_{kj}), \tag{4}$$

where $\Gamma_{kj} = \delta_{jk}\gamma_j$, the subscripts i, j, k correspond to the states, Γ_{ik} indicates the spontaneous radiation attenuation

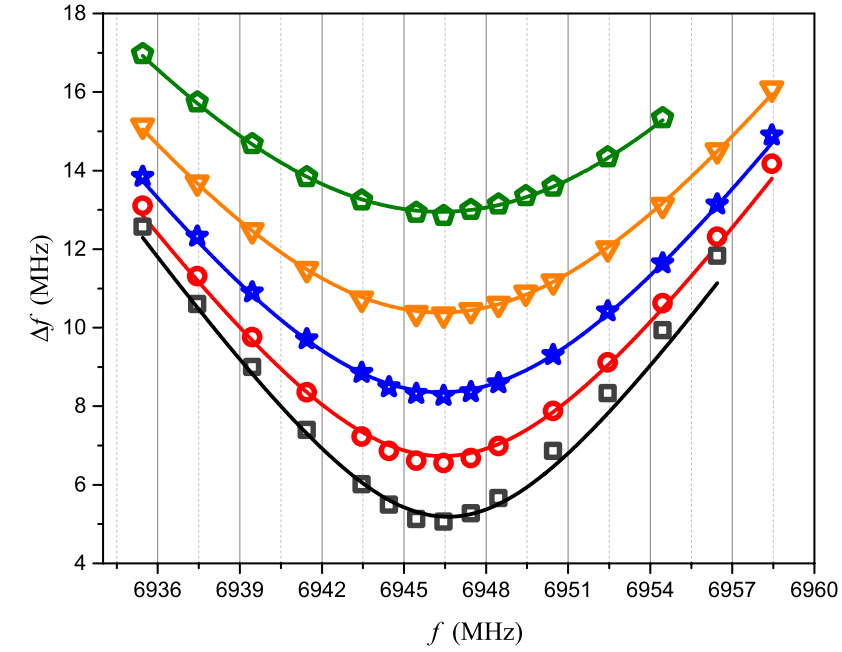

(a)

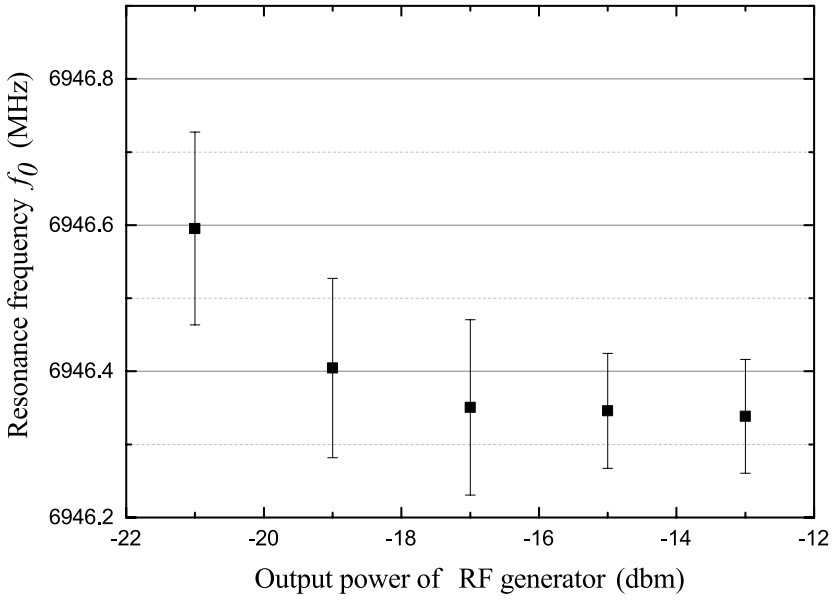

(b)

Figure 3. (a) The AT splitting interval versus the RF E-field frequency with the applied power of −13 dbm (black square), −15 dbm (red circle), −17 dbm (blue star), −19 dbm (orange angle), −21 dbm (olive pentagon), respectively. The black solid lines are the fitting curves using equation (2). (b) The fitting resonance frequency f_0 versus the output power of the RF generator.

from $|i>$ to $|k>$, and the parameter γ_j is the decay rate for the various states. Here, ρ_{kj} is the coherence between states k and j. Solving the probability density equations can obtain ρ_{21}, to obtain the dispersion and absorption spectra of Rydberg EIT including the RF E-field. The imaginary part of the ρ_{21} can be calculated as

where

$$a_1 = \frac{1}{2}\Omega_M^2\gamma_{12} - 2\delta\left(\gamma_{13}\Delta_p + \gamma_{12}\left(\Delta_p + \Delta_c\right)\right) + 2\gamma_{14}\left(\frac{\Omega_c^2}{4} - \Delta_p\left(\Delta_p + \Delta_c\right) + \gamma_{12}\gamma_{13}\right),$$

$$\mathrm{Im}\left(\rho_{21}\right) = \Omega_p\frac{2\left(\gamma_{14}\left(\Delta_p + \Delta_c\right) + \gamma_{13}\delta\right)a_2 + \left(\frac{1}{4}\Omega_M^2 - \left(\Delta_p + \Delta_c\right)\delta + \gamma_{13}\gamma_{14}\right)a_1}{a_1^2 + 4a_2^2}, \tag{5}$$

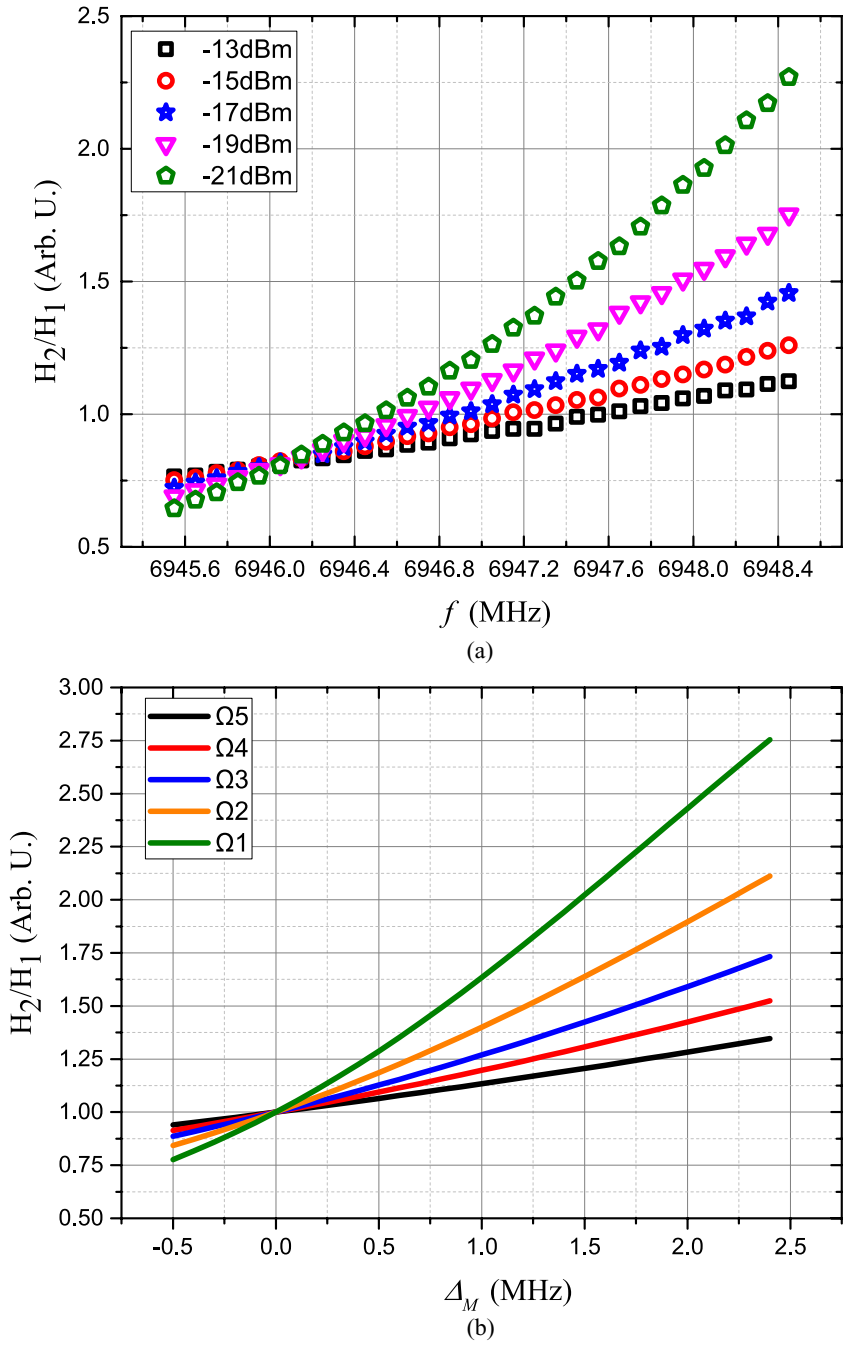

Figure 4. (a) The measured height ratio of AT splitting peaks versus the RF E-field frequency. (b) Theoretical simulation curves.

$$a_2 = \frac{1}{4}\Omega_M^2\Delta_p + \delta\left(\frac{\Omega_c^2}{4} - \Delta_p\left(\Delta_p + \Delta_c\right) + \gamma_{12}\gamma_{13}\right) + \gamma_{14}\left(\gamma_{13}\Delta_p + \gamma_{12}\left(\Delta_p + \Delta_c\right)\right),$$

$$\delta = \Delta_p + \Delta_c + \Delta_M \text{ and } \gamma_{ij} = (\Gamma_i(i-1) + \Gamma_j(j-1))/2(i,j = 2,3,4).$$

We select reasonable experimental parameters to fit the height ratio of the splitting peaks by using equation (5). Here, we set $\Delta_p = 0$, $\gamma_{12} = 2\pi \times (5.2$ MHz), $\gamma_{13} = 2\pi \times (0.1$ MHz), $\gamma_{14} = 2\pi \times (0.1$ MHz), $\Omega_p = 2\pi \times (1.4$ MHz) and $\Omega_c = 2\pi \times (1.4$ MHz): γ_{12} is the decay rate of $6P_{3/2}$; and γ_{13} and γ_{14} are the decay rates of Rydberg states accounting for the large collision cross-section of Rydberg atoms [1]. Here, Ω_M are the variation values from the splitting for different detuning in figure 3. In figure 4(b), all curves cross at the resonance frequency ($\Delta_M = 0$) in which the relative height ratio equals 1. It is reasonable to conclude that the RF E-field causes the resonant frequency shift and the height ratio of AT splitting can offer the reference to calibrate the resonance frequency for different RF E-field strengths. For the frequency shift introduced by the splitting fitting in figure 3 and height ratio in figure 4, the introduced error of the E-field strength using equation (2) is smaller than 1% for the weak field measurement.

Furthermore, we investigate the effect of the detuning of the probe field on the RF E-field measurement. The RF E-field

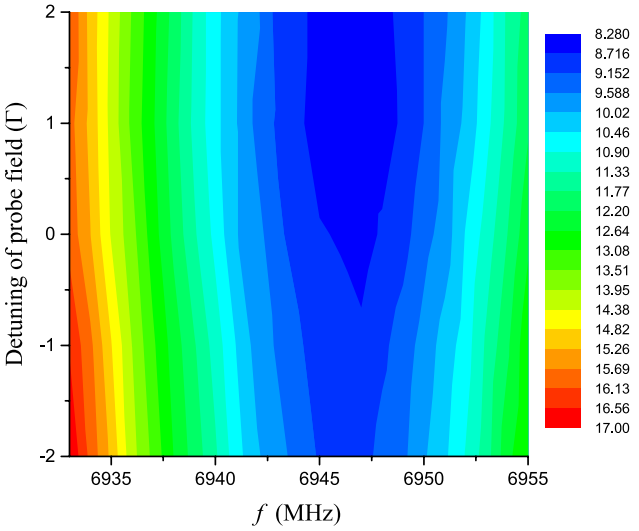

Figure 5. The AT splitting of EIT for the probe detuning and RF frequency. Γ is the natural linewidth of $6P_{3/2}$.

strength is about 31 mV cm^{-1} according to the calculation using the splitting of the resonant frequency. The frequency of the probe laser varies to the resonance frequency fp of transition $6S_{1/2}$, $F = 4 \leftrightarrow 6P_{3/2}$, $F' = 5$, $f\mathrm{p} \pm \Gamma$ and $f\mathrm{p} \pm 2\Gamma$, where Γ is the natural linewidth of $6P_{3/2}$. Figure 5 shows the AT splitting measurement versus the detuning of the probe laser and the RF E-fields. The minimum splitting interval indicates the resonance for both the probe laser and the RF field. The detuning of the probe laser will produce a measurement error smaller than 6.3% in our experiments.

When the RF field is off-resonant with the Rydberg states, the splitting interval shows the asymmetric characteristic for the red detuning and blue detuning of the probe laser. While the probe laser is tuned on the blue side, the measurement deviation of the RF E-field strength is bigger than that which is measured when the probe laser is red detuning. Red detuning of the probe laser will produce more measurement deviation for the blue detuning RF E-field. The asymmetric characteristic is attributed to the asymmetric shift of hyperfine levels under the stray magnetic field around the vapor cell [21, 22].

In conclusion, we investigated the effect of the detuning frequency of adjacent Rydberg state transitions on the RF E-field metrology in a cascade four-level system in a room-temperature vapor cell. We demonstrated the dependence of both the splitting intervals and the height ratio of two splitting peaks on the RF E-field frequency. The frequency shifts of Rydberg transition induced by the RF E-field are investigated. Furthermore, we showed the effect of probe detuning on the RF E-field measurement. Red detuning of the probe laser will produce the asymmetric measurement deviation in the detuning RF E-field metrology.

Acknowledgments

This work was supported by the National Key Research and Development Program of China (Grant Nos. 2017YFA0304203 and 2016YFF0200104), the National Natural Science Foundation of China (Grant Nos. 61827824 and 91536110) and the Fund for Shanxi '1331 Project' Key Subjects Construction, Bairen Project of Shanxi Province, China.

References

[1] Gallagher T F 1994 *Rydberg Atoms* 4th edn (Cambridge: Cambridge University Press) p 11
[2] Zimmerman M L, Castro J C and Kleppner D 1978 *Phys. Rev. Lett.* **40** 1083
[3] Zimmerman M L, Littman M G, Kash M M and Kleppner D 1979 *Phys. Rev.* A **20** 2251
[4] Scully M O and Zubairy M S 1997 *Quantum Optics* 1st edn (Cambridge: Cambridge University Press) p 225
[5] Harris S E and Hau L V 1999 *Phys. Rev. Lett.* **82** 4611
[6] Hakuta K, Marmet L and Stoicheff B P 1991 *Phys. Rev. Lett.* **66** 596
[7] Ahmed E, Hansson A, Qi P, Kirova T, Lazoudis A, Kotochigova S, Lyyra A M, Li L, Qi J and Magnier S 2006 *J. Chem. Phys.* **124** 084308
[8] Piotrowicz M J, MacCormick C, Kowalczyk A, Bergamini S, Beterov L L and Yakshina E A 2011 *New J. Phys.* **13** 552
[9] Eisaman M D, André A, Massou F, Fleischhauer M, Zibrov A S and Lukin M D 2005 *Nature* **438** 837
[10] Höckel D and Benson O 2010 *Phys. Rev. Lett.* **105** 153605
[11] Fan H Q, Kumar S, Sedlacek J, Kübler H, Karimkashi S and Shaffer J P 2015 *J. Phys. B: At. Mol. Opt. Phys.* **48** 202001
[12] Sedlacek J A, Schwettmann A, Kübler H, Löw R, Pfau J P and Shaffer T 2012 *Nat. Phys.* **8** 819
[13] Sedlacek J A, Schwettmann A, Kübler J P and Shaffer H 2013 *Phys. Rev. Lett.* **111** 063001
[14] Fan H Q, Kumar S, Daschner R, Kübler J P and Shaffer H 2014 *Opt. Lett.* **39** 3030
[15] Holloway C L, Gordon J A, Schwarzkopf A, Anderson D A, Miller S A, Thaicharoen N and Raithel G 2014 *Appl. Phys. Lett.* **104** 244102
[16] Fan H Q, Kumar S, Sheng J T and Shaffer J P 2015 *Phys. Rev. Appl.* **4** 044015
[17] Simons M T, Gordon J A, Holloway C L, Anderson D A, Miller S A and Raithel G 2016 *Appl. Phys. Lett.* **108** 174101
[18] Holloway C L, Gordon J A, Schwarzkopf A, Anderson D A, Miller S A, Thaicharoen N and Raithel G 2014 *IEEE Trans. Antennas Propag.* **62** 6169
[19] Wu J, Ji Z A, Zhang Y, Wang L, Zhao Y, Ma J, Xiao L and Jia S 2011 *Opt. Lett.* **36** 2038
[20] Kwak T, Jeong Y S, Lee H M and Moon H S 2016 *Opt. Commun.* **380** 168
[21] Bao S X, Yang W G, Zhang H, Zhang L J, Zhao J M and Jia S T 2015 *J. Phys. Soc. Japan* **84** 104301
[22] Bao S X, Zhang H, Zhou J, Zhang L J, Zhao J M, Xiao L T and Jia S T 2016 *Phys. Rev.* A **94** 043822